The American Association of Petroleum Geologists Bulletin
V. 77, No. 3 (March 1993), P. 402–413, 11 Figs., 3 Tables

Predicting Depths of Gypsum Dehydration in Evaporitic Sedimentary Basins[1]

E. Craig Jowett,[2] Lawrence M. Cathles III,[3] and Bruce W. Davis[4]

ABSTRACT

The conversion of gypsum to anhydrite upon burial and heating is accompanied by about a 39% volume decrease, a four-fold increase in thermal conductivity, and consumption of heat. Accurate "back-stripping" of an evaporite basin and tracking its thermal evolution requires a knowledge of the depth of the gypsum-anhydrite transition. This depth depends on temperature, fluid pressure, lithostatic pressure, and activity of water in the pore fluid. Using a finite-difference heat-conduction program, we have determined the depths of transition for gypsum in evolving basins beneath commonly associated sediments and in several tectonic environments represented in the program by different basal heat flows and sedimentation rates. The activity of water is kept at 0.93 (precipitation of gypsum from seawater). All physical properties are recalculated at each time step as temperature increases and porosity decreases with burial. (An algorithm for calculating thermal conductivities using parallel-series mixtures is presented.) The modeling results show that overlying lithologies and the tectonic environment are two important factors. Gypsum converts to anhydrite at shallow depths (~400 m) when overlain by poor conductors like shale or gypsum in a rift environment, and at great depths (hypothetically >4 km) when overlain by good conductors like salt in a stable cratonic region. Sedimentation rate and the transient "heat sink" effect of the endothermic reaction have little effect on transition depth.

[1]Manuscript received February 25, 1991; revised manuscript received March 27 1992; final acceptance April 21, 1992.

[2]Department of Earth Sciences, University of Waterloo, Waterloo, Ontario N2L 3G1, Canada.

[3]Department of Geological Sciences, Cornell University, Ithaca, New York 14853-1504.

[4]Chevron Oil Field Research Company, P.O. Box 446, La Habra, California 90633-0446.

This research was funded by the Natural Sciences and Engineering Research Council of Canada (grant URF0037724 to Jowett) and by the Donors of The Petroleum Research Fund administered by the American Chemical Society (grants 19767-AC2 to Cathles and 23806-AC8 to Jowett). We acknowledge Chevron Oil Field Research Company for permission to publish the parallel-series algorithm in the Appendix. We appreciate the helpful criticism of B. C. Schreiber, J. H. Doveton, W. D. Wiggins, and V. V. Palciauskas.

This paper is a contribution to IGCP Project 254, "Metalliferous Black Shales."

INTRODUCTION

When analyzing or modeling a sedimentary basin composed mainly of clastic rocks, the original basin thickness and shape can be reconstructed by decompacting or "back-stripping" the various formations through time (e.g., Sclater and Christie, 1980). In an evaporite basin with significant anhydrite, however, the normal decompaction techniques cannot be used. The problem is that gypsum, assumed here to be the dominant primary sulfate sediment (Murray, 1964; Rouchy et al., 1987; Schreiber, 1978), dehydrates to anhydrite rather abruptly upon reaching a specific depth and temperature. The reader is referred to Sonnenfeld (1984) for a discussion of the geologic evidence relating to conversion depths.

Knowledge of this conversion depth is essential for stratigraphic reconstructions (because of the ~39% decrease in sediment thickness) and for heat-flow and fluid-flow modeling by computer (because of the four-fold increase in thermal conductivity). For example, in a simple sensitivity test with a basal heat flow of 2×10^{-6} cal/cm^2/s (2 heat flow units, or HFU), the thermal gradient through anhydrite is found to be about 18°C/km, whereas with gypsum, it is about 63°C/km. Using the wrong lithology produces large errors. For example, using 500 m of cumulative anhydrite beds instead of 806 m of decompacted gypsum (Figure 1) produces about a 42°C discrepancy at the base of the evaporite unit. This error would significantly alter the calculated thermal structure of the basin, and potential hydrocarbon source beds could be ignored. In addition, use of siliciclastic sediments which do not compact as the basin model evolves also creates significant errors. For example, the thermal gradient through nonporous, noncompacting shale is about 29°C/km, compared to about 44°C/km through a dewatering shale with an initial 40% porosity, result-

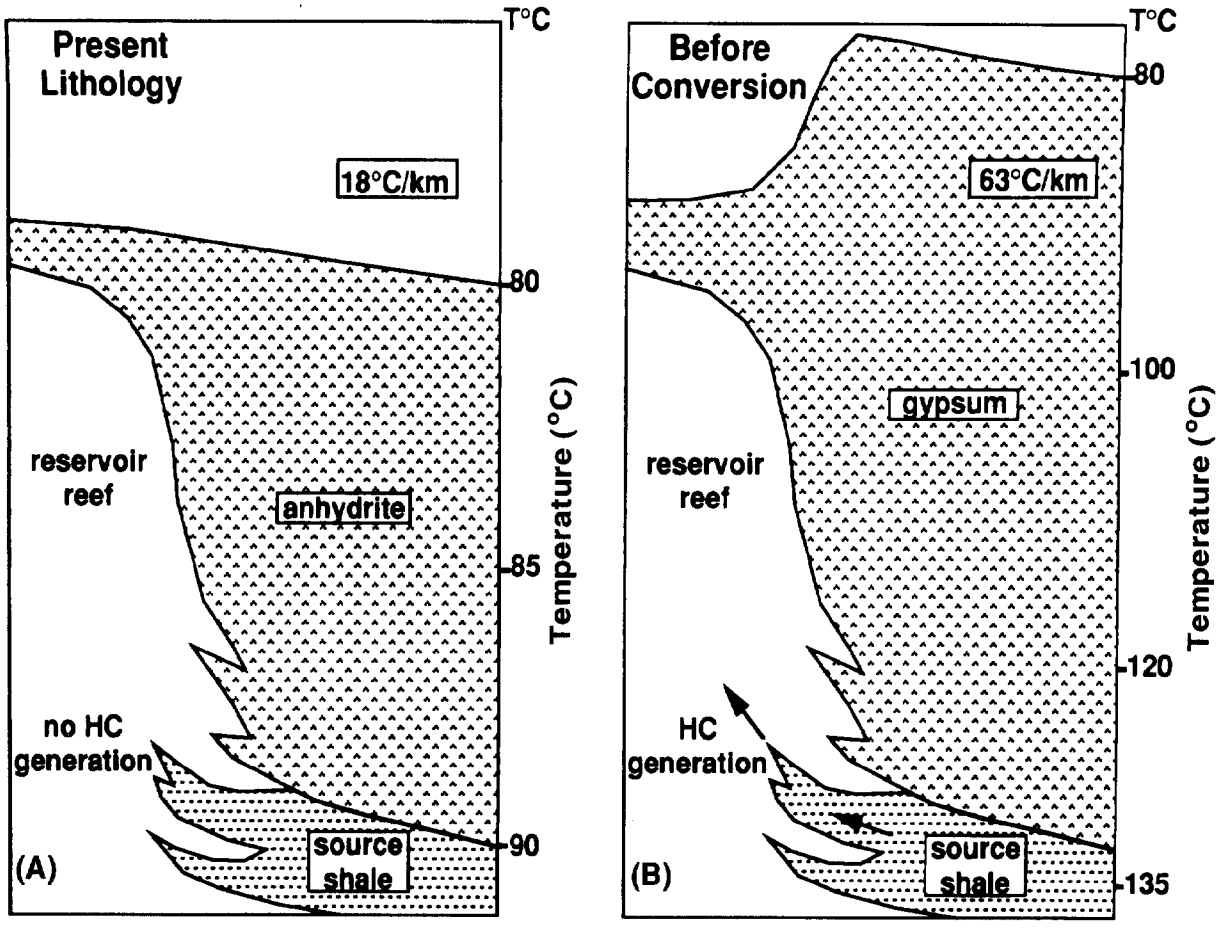

Figure 1—(A) In an evaporite basin containing a cumulative thickness of 500 m of anhydrite, the calculated paleothermal structure suggests that the underlying source shale did not enter the "oil window." (B) However, in a decompacted basin before gypsum-anhydrite conversion, the source beds generate hydrocarbons because the low thermal conductivity of the gypsum increases the thermal gradient.

ing in a potential error of 15°C in a 1000-m thick stratigraphic section.

This paper describes a method to predict the conversion depth of a gypsum bed in a given stratigraphic column using a one-dimensional finite-difference program, and shows that, once the physical parameters of the environment are set, the conversion depth depends primarily on (1) lithology of the overlying sediments and (2) the plate-tectonic environment. The compaction mechanics described are also useful for general heat flow modeling in siliciclastic basins that are growing and compacting.

TEMPERATURE OF GYPSUM-ANHYDRITE CONVERSION

Gypsum converts to anhydrite according to equation (1) upon reaching a temperature ($T_{gp\text{-}an}$) which varies according to the physical and geochemical environment of the gypsum:

$$CaSO_4 \cdot 2H_2O \rightarrow CaSO_4 + 2H_2O \qquad (1)$$

The heat of reaction (ΔH_r) in this endothermic reaction at 25°C is about 4 kcal/mol anhydrite formed (Hardie, 1967). In their theoretical and experimental studies of the relative stability fields of gypsum and anhydrite, MacDonald (1953), Hardie (1967), and Hanshaw and Bredehoeft (1968) determined that the primary physical controls of $T_{gp\text{-}an}$ are (1) the activity of water in the pore fluid and (2) the pore fluid pressure.

Activity of Pore Water

As the activity of water (α_{H2O}) in the pore fluid increases, equation (1) is retarded, gypsum becomes more stable, and more energy must be added to the

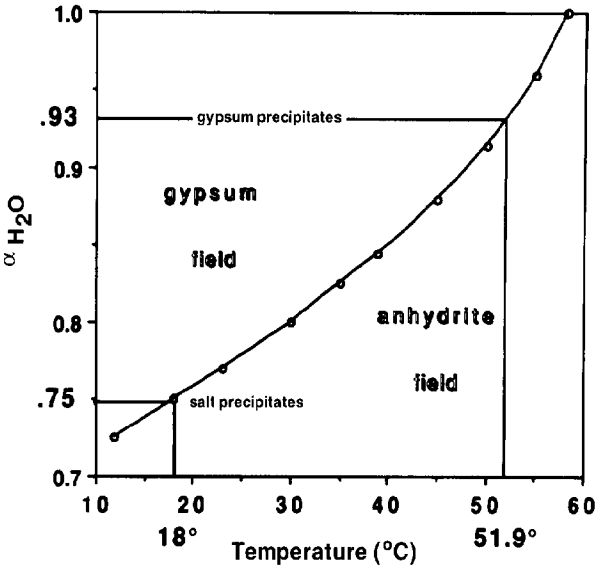

Figure 2—Relationship between the activity of water (α_{H2O}) and the temperature at which gypsum converts to anhydrite ($T_{gp\text{-}an}$) under laboratory conditions. (Data points from Table 3 in Hardie, 1967.)

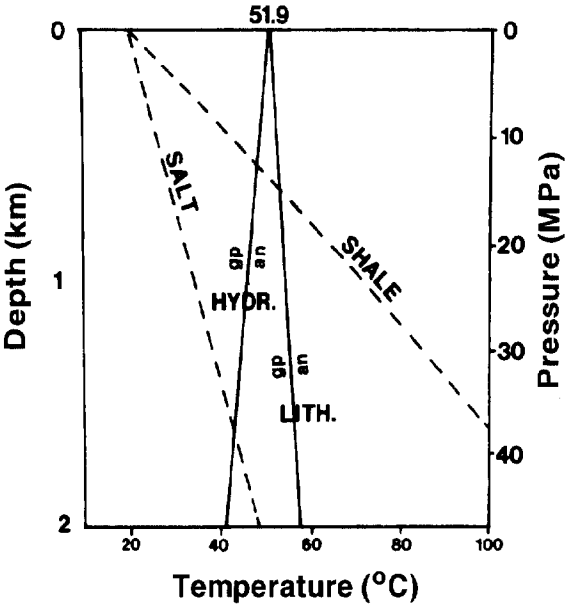

Figure 3—Depth relationship of $T_{gp\text{-}an}$ for hydrostatic and lithostatic fluid-pressure regimes and below shale insulator vs. salt conductor. Primary anhydrite can form at temperatures less than about 52°C if α_{H2O} decreases (e.g., NaCl precipitates). Conversion to anhydrite occurs where the $T_{gp\text{-}an}$ line intersects the geothermal gradient in the overlying rock. Early conversion to anhydrite results if gypsum is buried in a rift zone (high heat flow) or is overlain by a sediment of low thermal conductivity (shale). α_{H2O} = 0.93, ρ_s = 2.4 g/cm^3, 2 HFU. After MacDonald(1953), Hardie (1967), and Hanshaw and Bredehoeft (1968).

system to produce anhydrite (Figure 2). With an α_{H2O} of 0.93, the activity at which gypsum precipitates from seawater (Hanshaw and Bredehoeft, 1968), $T_{gp\text{-}an}$ is about 52°C, but when halite (NaCl) is precipitated from more saline brines, the α_{H2O} is 0.75, and $T_{gp\text{-}an}$ is about 18°C (Hardie, 1967). Therefore, synsedimentary anhydrite could be expected only if surface temperatures are high and if halite is a coeval phase (e.g., anhydrite nodules found on the coast of the United Arab Emirates and documented by Shearman, 1963). Certainly anhydrite would be stable if sylvite (KCl) is a coeval phase formed from brines with an even lower α_{H2O} (Hardie, 1967). However, we set α_{H2O} = 0.93, the activity at which gypsum is precipitated from seawater. A correction for lower α_{H2O} can be made by simply determining the initial temperature for a particular α_{H2O} (Figure 2) and then subtracting the difference from 51.9°C from the temperatures determined in our modeling results.

α_{H2O} can be estimated from compositions of the surrounding lithologies. For example, if a gypsum bed (now anhydrite) shows no evidence of coeval salt precipitation and is associated with normal siliciclastic sediments such as shale or sandstone, then one can assume that the pore water closely reflects the original formation water (e.g., $\alpha_{H2O} \approx 0.93$ for seawater). If evidence of coeval or early diagenetic salt cement is apparent, then an α_{H2O} of about 0.75 would be more appropriate, and the depth of conversion would be much shallower. These assumptions have to be made on the basis of geologic evidence.

Pore Fluid Pressure

When gypsum converts to anhydrite (equation 1), the molar volume of the solid phase decreases by ΔV_s = -28.37 cm^3/mol of anhydrite formed, corresponding to a volume decrease of about 39% (Zen, 1965; Hanshaw and Bredehoeft, 1968). However, there is a corresponding increase in molar volume of ΔV_f = 36 cm^3 for the 2 mol of water formed. Because the pressures on the fluid (P_f) and solid (P_s) phases are different, the molar entropy change (S) and molar volume change (ΔV) are related by equation (2) (Hanshaw and Bredehoeft, 1968):

$$dP_s/dT = S/(\Delta V_s + V_f\, dP_f/dP_s) \qquad (2)$$

The entropy change is $\Delta S = -135.84 + 65.17\log_{10}T - 0.043T$ (Hardie, 1967), where T is temperature in kelvins. In a hydrostatic fluid-pressure regime (e.g., gypsum in sandstone), the released water escapes from the immediate area and the overburden pressure is taken up by the solid phases only, thus favor-

ing the denser solid phase, anhydrite. In this case, $dP_f/dP_s = \rho_f/\rho_s$ = about 0.4, and the slope of dP_s/dT on a P-T plot is negative (positive slope on a D-T plot such as Figure 3). $T_{gp\text{-}an}$ actually decreases with depth, and gypsum converts early at a shallow depth (Figure 3). If the water cannot escape, the pore fluids become geopressured in a lithostatic pressure regime (e.g., sealed in below salt), and the overburden pressure is taken up by both the fluid and the solid phases. In this case, P_f approaches P_s, dP_f/dP_s approaches unity, and the slope of dP_s/dT becomes positive (Hanshaw and Bredehoeft, 1968). $T_{gp\text{-}an}$ increases with depth, and conversion to anhydrite will occur at a greater depth than the hydrostatic case for a given geothermal gradient (Figure 3). Whether the dominant pore-fluid pressure regime is hydrostatic or lithostatic can be estimated from the hydraulic conductivity and the extent of coverage of overlying rock. When this estimate cannot be made with confidence, conversion depths can be calculated for hydrostatic and lithostatic extremes. However, Hanshaw and Bredehoeft (1968) calculated that lithostatic conditions can only be maintained for a "geologic instant" within the gypsum bed, even if the confining beds have hydraulic conductivities as low as 10^{-10} cm/s, a value that includes all rocks except very tight shales (Freeze and Cherry, 1979). In our simulations, $T_{gp\text{-}an}$ and conversion depth are calculated for both pressure regimes.

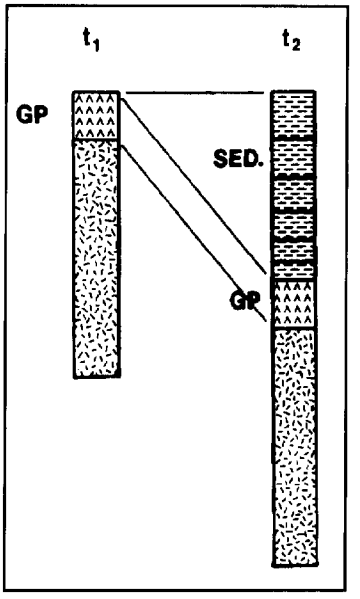

Figure 4—Schematic diagram of the simulation. The initial section has a basal 20-m layer of gypsum on 1 km of basement. With each time step, a 20-m increment of sediment is added and the underlying sediments are compacted; new porosities, new physical properties, and new temperature profile are calculated.

DEPTH OF GYPSUM-ANHYDRITE CONVERSION

Heat Flow Equation

The temperature of gypsum-anhydrite conversion ($T_{gp\text{-}an}$) is reached at a shallow depth in a basin with a high geothermal gradient ("shale" line in Figure 3) compared to one with a low geothermal gradient ("salt" line in Figure 3). The gradient is an effect of the basal heat flow and the thermal conductivity of the sedimentary rocks. The controls of the geothermal gradient can be seen in the equation for steady-state one-dimensional conductive heat flow:

$$q = K\Delta T/\Delta z + Q \qquad (3)$$

where q is heat flow density through the water-saturated sediment, K is thermal conductivity in the vertical direction, $\Delta T/\Delta z$ the geothermal gradient (with z being the depth below surface), and Q is radioactive heat production. The top boundary condition is ambient average T; the bottom boundary condition is the heat flux from the basement and mantle. The temperature of a bed of gypsum varies directly with the heat flow introduced to the bed from below and inversely with the thermal conductivity of the overlying sedimentary column. Therefore, gypsum which lies below a thermal insulator such as organic-rich shale or in a high heat-flow area such as a rift basin should convert to anhydrite earlier in its history than gypsum below a thermal conductor such as salt or in a cold stable continental interior.

SIMULATING A COMPACTING BASIN

Computer Program

A one-dimensional finite-difference program based on equation (3) was written to simulate the burial of a gypsum bed in a compacting sedimentary basin and to determine the depth of $T_{gp\text{-}an}$ under a variety of geologic conditions. In the simulation, a 20-m increment of gypsum on 1000 m of noncompacting "basement" is buried with 20-m increments of sediment added at subsequent time steps (Figure 4). The calculations performed at each time step by the program are indicated in Table 1.

Initial Physical Parameters

Basal heat flow, surface temperature, and sedimentation rate are initially set and remain constant for the entire simulation. Heat capacity, heat production, and thermal conductivity are set for the basement and gypsum increments, and the thermal conductivity is continuously updated as the basin evolves. For the overlying sediments, the initial porosity (ϕ_0) and the compaction factor (c) (see equation 4 below) are set for the entire simulation, but the physical parameters of heat capacity, heat production, density, and thermal conductivity are set for the solid rock matrix only, and are varied during the simulation as the sediment compacts and pore fluids are lost.

Table 1. Flow Sequence of Compacting Basin Program

Add 20-m increment of shale on gypsum layer
Compact shale from initial porosity (ϕ_0)
Calculate for each increment:
  new porosity (ϕ_i)
  new increment-thickness from ϕ_i
  new heat capacity, heat production, density from ϕ_i
  new thermal conductivity from ϕ_i and T_i
  new T_i of each increment in section
  new $T_{gp\text{-}an}$ given gypsum depth & density of overlying strata
Compare gypsum layer T_{gp} with $T_{gp\text{-}an}$
Repeat until gypsum layer $T_{gp} = T_{gp\text{-}an}$

Compaction of Siliciclastic Sediments

For the purposes of this study, rock salt and gypsum sediments laid down on the initial gypsum layer are assumed to be nonporous and noncompacting because of their crystalline framework and rapid loss of initial pore space (Sonnenfeld, 1984). However, the siliciclastics used (sandstone and shale) are compacted at each time step using the relationship,

$$\phi_i = \phi_0 e^{-cz} \quad (4)$$

where ϕ_0 is initial porosity of the sediment, c is the compaction factor, and z is depth (in km). For sandstone, $\phi_0 = 0.49$ and $c = 0.27$ to be consistent with Sclater and Christie (1980). For shale, measured porosities of shale in the shaly section of the South Caspian basin (Bredehoeft et al., 1988) were used. The upper 3.25 km of the basin appeared to compact smoothly as an integral unit, and a best-fit curve of these data resulted in $\phi_0 = 0.40$ and $c = 0.27$ (Figure 5).

Although carbonate rocks are an important component of evaporite basins, they are not included in this study because of the difficulty in estimating the 20–35% compaction due to pressure solution (Bathurst, 1975). A very rough approximation, however, can be obtained by using the results for sandstones because the thermal conductivities are within the same range.

As sediment is added and the earlier sediments compacted, increment thickness (D_i) (used for finite-difference computation), heat capacity of the sediment (C_i), heat production of the sediment (Q_i), and sediment density (ρ_i) are recalculated:

$$D_i = D_0 (1 - \phi_0)/(1 - \phi_i) \quad (5)$$

$$C_i = C_r(1 - \phi_i) + C_f\phi_i \quad (6)$$

$$Q_i = Q_r(1 - \phi_i) \quad (7)$$

$$\rho_i = \rho_r(1 - \phi_f) + \rho_i\phi_i \quad (8)$$

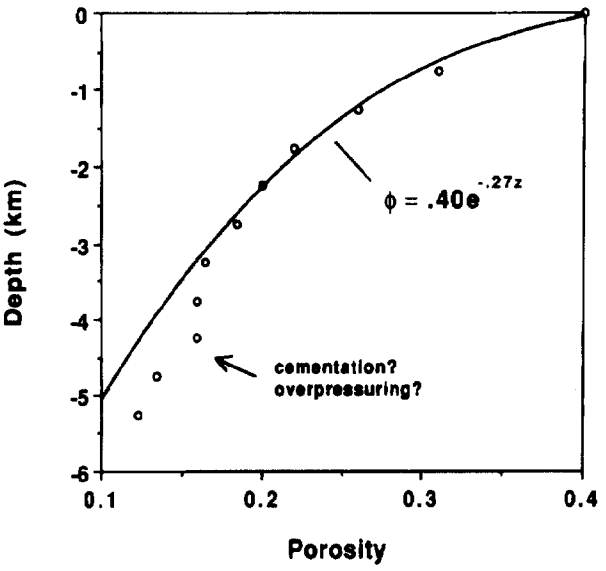

Figure 5—Measured porosity data in shale in the shaly section of the South Caspian basin. Best-fit curve to consistent data in upper 3.25 km results in $\phi_0 = 0.40$ and $c = 0.27$ (area III in Bredehoeft et al., 1988).

where C_r is the heat capacity of the rock matrix, C_f is the heat capacity of the pore fluid, Q_r is the heat production of the rock matrix ($Q_f = 0$), ρ_r is the density of the rock matrix, and ρ_f is the density of the pore fluid (= 1).

THERMAL CONDUCTIVITY CALCULATION

The best method of calculating the bulk thermal conductivity of a rock formation from its rock matrix constituents and its porosity has been the object of much discussion, but a mixture of parallel and series elements (modified Maxwell model) is preferred by Roy et al. (1981) and Beck (1988). Davis (1984) advanced this technique further by first calculating the rock matrix conductivity using a proportion of parallel and series elements, and then mixing that conductivity with the pore fluid using another proportion (see the Appendix). At both stages, the effect of temperature is also calculated. We have adopted Davis' (1984) method, which has been satisfactorily fitted to data in several case studies. Both the rock and water thermal conductivity are functions of temperature and porosity. Temperature and porosity change with depth as described by equations (3) and (4).

Parallel and Series Elements

The two extremes of conductivities, K_P and K_S, are depicted in Figure 6. In this example, the bulk

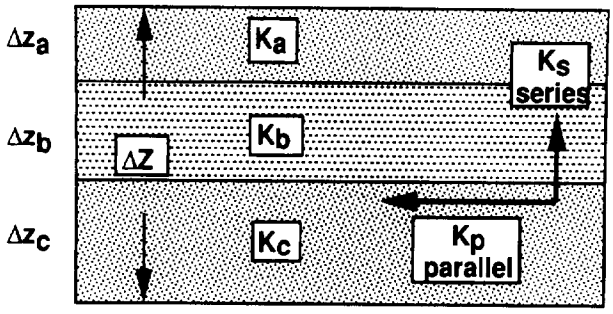

Figure 6—Parallel and series elements of thermal conductivity showing the extreme values of K_p and K_s in an anisotropic medium. A rock matrix can be characterized as a mixture of these two extremes. The whole rock (matrix and pore fluid combined) can likewise be characterized by mixing theory.

thermal conductivity of the formation in the vertical direction can be shown to be

$$K_S = \Delta z/(\Delta z_a/K_a + \Delta z_b/K_b + \Delta z_c/K_c), \quad (9)$$

and in the horizontal direction to be

$$K_P = K_a\Delta z_a/\Delta z + K_b\Delta z_b/\Delta z + K_c\Delta z_c/\Delta z, \quad (10)$$

where K_a, z_a, etc. are conductivities and thicknesses of individual layers, respectively, and z is the total thickness (Figure 6).

Rock Matrix Conductivity

The rock matrix or grain conductivity (K_g) is first calculated at room temperature (298 K) from the individual mineral constituents, using a 30:70 mixture of parallel and series elements (see the Appendix):

$$K_g = 0.3\Sigma x_iK_i + 0.7\{\Sigma(x_i/K_i)\}^{-1} \quad (11)$$

where x_i is the proportion and K_i is the thermal conductivity of each constituent mineral at 298 K. The effect of temperature on K_g is calculated using

$$K_g(T) = \{K_g^{-1}(2.412 - 0.0818T^{0.5}) + 0.01724T^{0.5} - 0.2978\}^{-1} \quad (12)$$

(Conductivity units for these calculations are mcal/s/cm/K.) For our study, generic sandstone and shale are used (average compositions are taken from Clark, 1982). The grain conductivities at 25°C for the sandstone and shale are .0145 and .0075 cal/s/cm/K, respectively (Table 2).

Pore Fluid Conductivity

The conductivity of the pore water as a function of temperature is

$$K_f(T) = 2.231(T/T_o)^{1.5} - 0.8812(T/T_o)^{2.5}T_o = 273.2 \text{ K} \quad (13)$$

Whole Rock Conductivity

The water-saturated rock conductivity is then calculated using a 50:50 mixture (Appendix):

$$K_R(T) = 0.5\{\phi K_f + (1 - \phi)K_g\} + 0.5\{\phi/K_f + (1 - \phi)/K_g\}^{-1} \quad (14)$$

where K_f, K_g, and ϕ refer to properties of each sediment increment. The thermal conductivities of the lithologic section after the basal gypsum layer is buried by about 2500 m of shale are depicted in Figure 7. The conductivity of the noncompacting basement rock decreases in value with increasing temperature (depth), whereas the conductivity of the noncompacting gypsum bed actually increases slightly with increasing temperature (effect of equation 12 on initially low conductivities). The conductivity of the compacting shale, on the other hand, increases with increasing depth because of the constant loss of low-conductivity pore water and the relative increase of high-conductivity rock matrix. The sediment eventually becomes less conductive with depth as pore fluid is exhausted and temperature becomes the controlling factor (Figure 8).

DEPTH PREDICTIONS

Model Results

The predicted depths of the gypsum-anhydrite transition ($D_{gp\text{-}an}$) vary considerably with the lithology of the overlying sediment and with the value of basal heat flow (Figure 9). Basal heat flow values vary with tectonic environment. The stable continental interior of North America is characterized by heat flow values of 1.0–1.5 HFU, whereas rift zones such as the Cenozoic Basin and Range province in the western United States and the Alpine foreland rifts of Europe contain values greater than 2.0 HFU (Blackwell, 1978; Jowett and Jarvis, 1984; Jowett, 1991).

Present-day heat flow values in petroliferous basins do not necessarily reflect the anomalously high heat-flow characteristic of active lithospheric extension when basin subsidence and sediment deposition are maximized (e.g., Jarvis, 1984). For example, active rifts in the Basin and Range pro-

Table 2. Physical Properties of Rock Units Used

Mineral	Conductivity*	Volume Fraction Sandstone	Shale	Gypsum	Anhydrite	Salt
Dolomite	0.0132	0.015	0.015	–	–	–
Calcite	0.0086	0.015	0.015	–	–	–
Quartz	0.0184	0.837	0.202	–	–	–
Illite-Mica	0.0055	0.082	0.505	–	–	–
Chlorite	0.0122	–	0.071	–	–	–
Kaolinite	0.0066	–	0.071	–	–	–
Plagioclase	0.0050	0.026	0.061	–	–	–
K-feldspar	0.0057	0.026	0.061	–	–	–
Gypsum	0.0030	–	–	1.00	–	–
Anhydrite	0.0122	–	–	–	1.00	–
Halite	0.0154	–	–	–	–	1.00
Rock Matrix Conductivity*		0.0145	0.0075	0.0030	0.0122	0.0154
at 100°C		0.0108	0.0068	0.0032	0.0097	0.0112
at 30% porosity		0.0073	0.0045	–	–	–
Rock Matrix Heat Capacity**		0.50	0.50	0.568	0.339	0.443
Radiogenic Heat Production†		2.0	2.5	0.0	0.0	0.0

*cal/s/cm/K.
**cal/cm^3.
†10^{13} cal/cm^3/s.

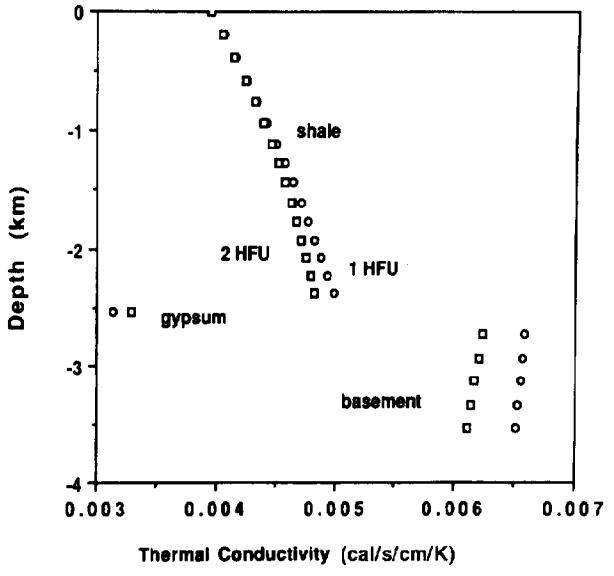

Figure 7—Thermal conductivities of the shale cover, gypsum bed, and basement at basal heat flow values of 1 and 2 HFU (10^{-6} cal/cm/s) calculated from equation (14). The shale conductivity increases with depth (temperature) because of the loss of low-conductivity pore fluid, whereas the nonporous basement rocks become less conductive with depth. Gypsum conductivity increases slightly with temperature, a characteristic of some insulators.

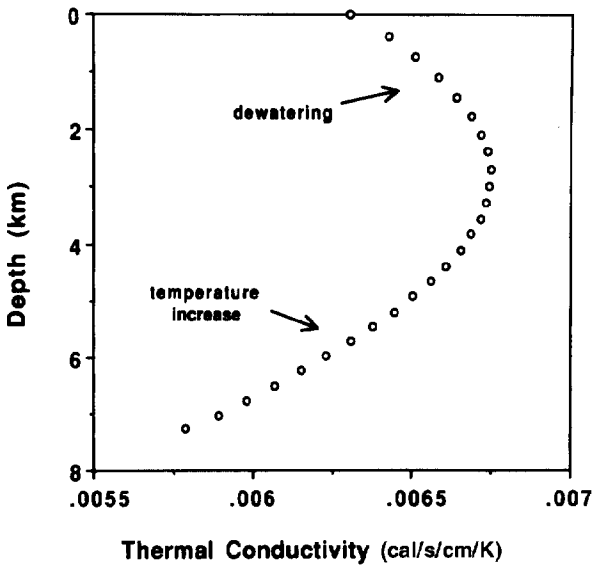

Figure 8—Grain conductivity decreases with temperature, but the effect of dewatering a compacting sandstone counteracts the temperature effect for several kilometers until the insulating pore fluid is expelled. Temperature then becomes the controlling factor if activity of pore water is consistent. Capping the sandstone with a shale seal to increase pore pressure delays dehydration of the gypsum bed.

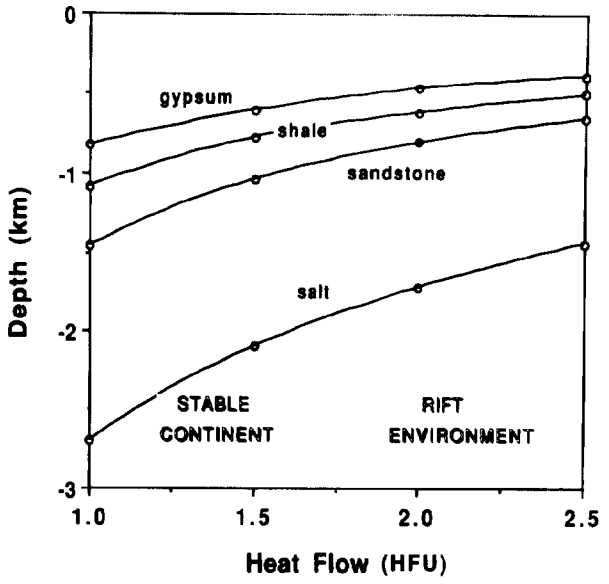

Figure 9—Depths of gypsum-anhydrite conversion ($D_{gp\text{-}an}$) in relation to lithologies of overlying sediment (gypsum, shale, sandstone, and salt) and to basal heat flow (tectonic environment). The α_{H2O} of the gypsum pore water is assumed to be 0.93. $D_{gp\text{-}an}$ is shallow when gypsum is overlain by thermal insulators like gypsum and shale and deeper below salt. $D_{gp\text{-}an}$ is shallower in regions of high heat flow such as rift zones, but deeper in cool continental interior basins.

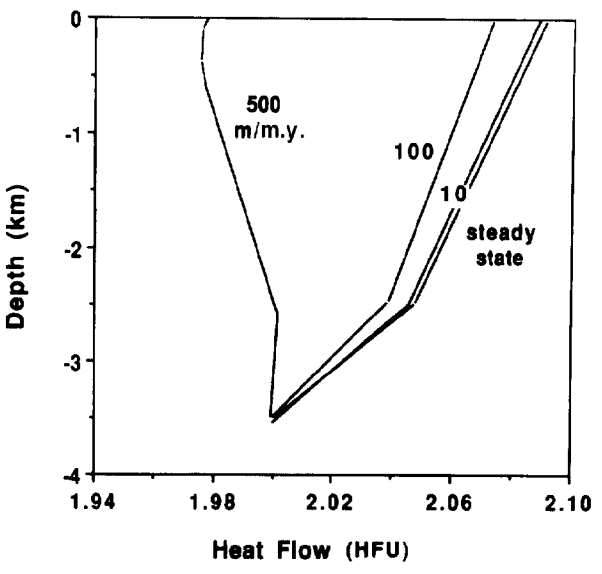

Figure 10—Transient heat-flow values with depth calculated from T between increments at different sedimentation rates (10, 100, 500 m/m.y.). The increase upsection for the steady-state reference and low-sedimentation conditions is due to radiogenic heat production (equation 3). However, very rapid addition of cold sediment (e.g., 500 m/m.y.) cools the upper section and increases $D_{gp\text{-}an}$.

Table 3. Depths (meters) of Gypsum-Anhydrite Conversion with Respect to Overlying Lithologies, Basal Heat Flow (HFU), and Hydrostatic (H) Vs. Lithostatic (L) Regimes*

		1.0 HFU	1.5 HFU	2.0 HFU	2.5 HFU
Gypsum	H	820	600	460	380
	L	1040	700	520	420
Shale	H	1085	770	610	500
	L	1490	945	700	555
Sandstone	H	1460	1035	800	650
	L	2230	1350	970	770
Salt	H	2700	2100	1720	1440
	L	–	3950	2780	2140

*All at 100 m/my sedimentation rate.

vince are characterized by values of more than 2.5 HFU, whereas those areas within the province that have been inactive for 17–20 m.y. have reverted back to about 1.5 HFU, similar to the continental interior base value (Blackwell, 1978). In this paper, basal heat flow values used to characterize stable continental interiors and active rift zones are 1.0 and 2.5 HFU, respectively.

In rift basins (2.5 HFU), the $D_{gp\text{-}an}$ varies five-fold (420 m vs. 2140 m) depending on whether the overlying lithology is, respectively, a thermal insulator like gypsum or a good conductor like salt. This ratio is magnified in continental interior basins because with low heat flow (1 HFU) the depression of the thermal gradient by the accumulating salt is great enough that the negative conversion gradient (Figure 3) prevents gypsum-anhydrite conversion under lithostatic pressure even at 5-km depth. Under hydrostatic pressure, the conversion depth is only 1040 m. This is an extreme case with an unrealistic thickness of salt, but it demonstrates the important control of overlying lithologies on thermal gradients, an effect also emphasized by Pollack and Cercone (1988). Sandstone is assumed to maintain hydrostatic pore-fluid pressures because compaction water can escape, whereas for shale, gypsum, and salt, a lithostatic pressure gradient is assumed, as shown in Figure 9. The computed depths for the alternative fluid pressure conditions are listed in Table 3.

These predictions of conversion depths are only as good as the geologic input. One important assumption is the α_{H2O} of the pore fluids at the time of depo-

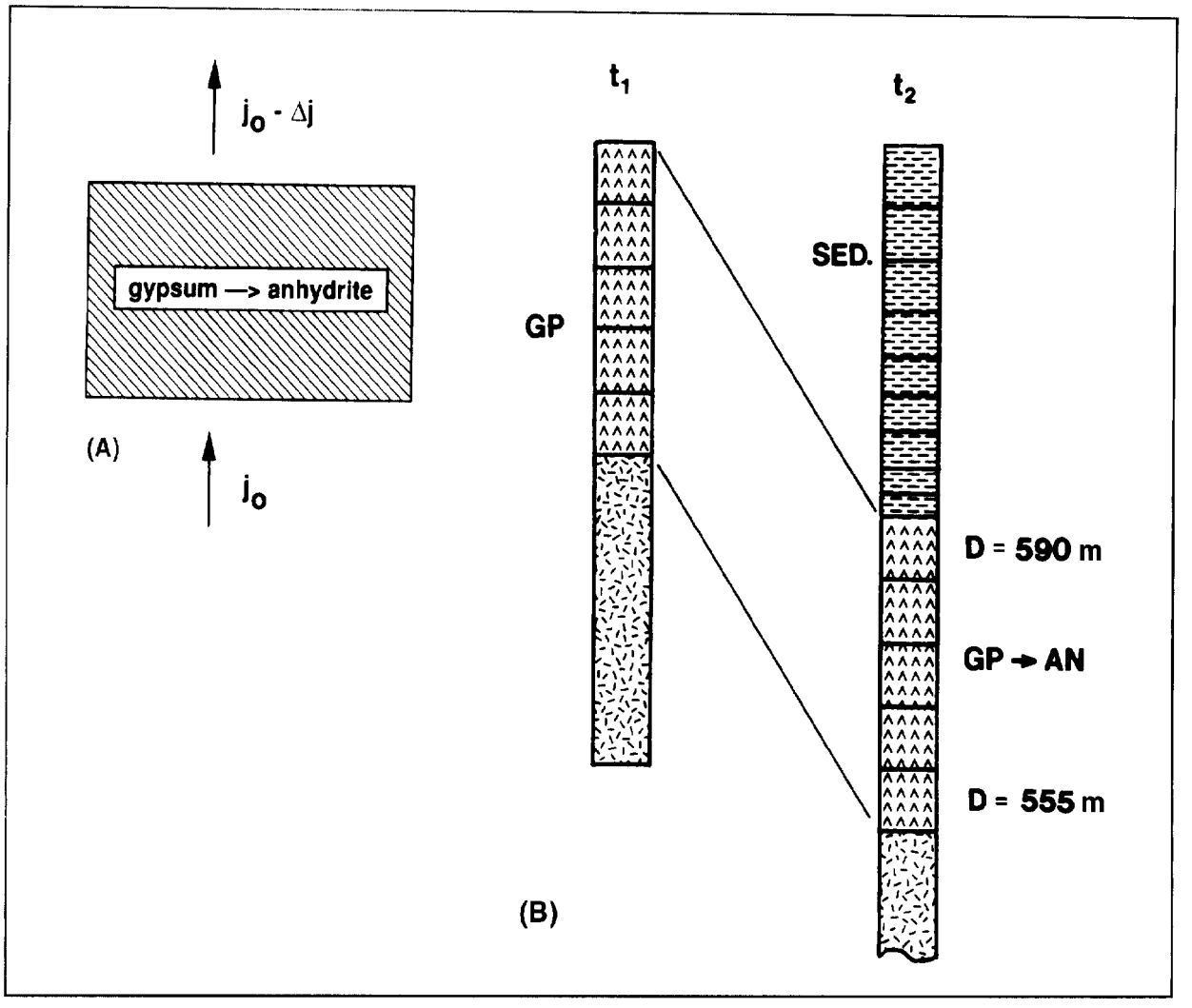

Figure 11—(A) The conversion of gypsum to anhydrite is an endothermic reaction or a heat "sink." Upper gypsum beds are sheltered from the full effect of the basal heat flow j_o, and therefore $D_{gp\text{-}an}$ is greater. (B) In a 200-m thick gypsum bed, the difference in $D_{gp\text{-}an}$ between the top and bottom due to the heat sink effect is only 35 m.

sition and early diagenesis. This value depends on the position of the anhydrite in the section and the lithology of associated rocks. In hydrologically closed systems, the water released by the reaction represented by equation (1) may slightly increase the α_{H2O} of adjacent pore water as dehydration continues. The close association of an anhydrite bed with salt or potash, its overall thickness, its position below a hydraulic seal, textural evidence of precursor gypsum, lithologies of overlying sediments, and the paleotectonic environment must be considered before depths can be estimated. Alternatively, when certain of these geologic controls are missing, upper and lower parameter bounds can be set arbitrarily and a range of depths of the gypsum-anhydrite transition can be calculated.

EFFECT OF SEDIMENTATION RATE

One can assume that if a gypsum bed is buried very rapidly by cold sediment, the gypsum-anhydrite transition will occur at a greater depth than if buried slowly and allowed to equilibrate. The effect of sedimentation rate is shown in Figure 10, in which the gypsum bed is buried by about 2500 m of shale at sedimentation rates of 10, 100, and 500 m/m.y. Heat flow is calculated from T between the sediment increments and compared to the steady-state profile (Figure 10). A rate of 10 m/m.y. is effectively the same as the steady-state profile (equivalent to no sedimentation), but with increasing rates, the upper sediments are added faster than they can heat up, and are in effect sheltered from the basal heat flow (Figure 10). However,

the effect was found to be small. In rift zones (2.5 HFU), the difference in $D_{gp\text{-}an}$ between rates of 100 and 500 m/m.y. is only about 20 m, or a single increment thickness, and in stable continental interiors (1 HFU), sedimentation rates of much more than 100 m/m.y. are necessary to produce a difference of more than 20 m, a sedimentation rate difficult to achieve in a quiet tectonic environment. These differences are not significant compared to other geologic uncertainties, and sedimentation rates can be ignored when predicting gypsum-anhydrite conversion depths.

GYPSUM-ANHYDRITE CONVERSION AS A HEAT SINK

Because the reaction represented by equation (1) is endothermic, during the time that the gypsum bed is being converted to anhydrite, heat is absorbed and overlying beds are sheltered from the full effect of the basal heat flow (Figure 11A). The upper beds in a thick sequence of gypsum "see" less heat than the lower beds (Hanshaw and Bredehoeft, 1968) because the basal heat flux is diminished by the endothermic gypsum to anhydrite conversion. Therefore the upper layers reach a greater depth before they reach their $T_{gp\text{-}an}$. The effect of this delay is tested for a 200-m thick bed of gypsum buried by shale (Figure 11B). As an increment of gypsum penetrates downward through the $T_{gp\text{-}an}$ isotherm, the amount of heat necessary to convert that nodal volume to anhydrite is calculated and subtracted from the heat flow, which then enters the increment directly above. The basal layer of gypsum in the 200-m section converts at about 570 m, whereas the upper increment does not convert until a depth of about 630 m, or about 10% deeper.

CONCLUSIONS

By constraining the parameters known to affect the depth of gypsum-anhydrite conversion ($D_{gp\text{-}an}$), the α_{H2O} of the pore water and the pore fluid pressure, estimates of $D_{gp\text{-}an}$ can be obtained and used to decompact an evaporitic basin for heat-flow and fluid-flow modeling purposes. These variables can be estimated from the composition of the immediate lithologies (α_{H2O}) and the hydraulic conductivity of the overlying lithologies (hydrostatic vs. lithostatic pore fluid pressure). By constraining these known variables, other factors such as rate of sedimentation, overlying rock type, basal heat flow, and the endothermic conversion reaction can be evaluated independently. Our modeling results show that gypsum converts to anhydrite at shallow depths (~400 m) when overlain by poor conductors like shale or gypsum in a rift environment, and at great depths (hypothetically >4 km) when overlain by good conductors like salt in a stable cratonic region. The rate of sedimentation and the endothermic conversion reaction ("heat sink") were found to have minor effects on the depth of conversion of gypsum to anhydrite.

APPENDIX: THERMAL CONDUCTIVITY OF SEDIMENTARY ROCKS

A method for estimating the bulk thermal conductivity of a sedimentary rock formation has been developed by one of us (Davis, 1984). Application of the method depends on a knowledge of the overall mineral composition of the sedimentary rock, rock porosity, matrix or grain thermal conductivities of the rock mineral constituents at 298 K, the temperature of the sedimentary formation, and the type of fluid saturations existing in the rock pore space.

Thermal Conductivity of a Heterogeneous Mixture

Combining rules predicting the effective thermal conductivity of heterogeneous mixtures have been the subject of scientific inquiry for more than a hundred years. As early as 1877, Schuhmeister used a weighted average of combining rules for series and parallel elements to predict the thermal conductivities of woven fabrics. Other workers, including Maxwell (1891), showed that the thermal conductivity of a composite medium must lie between the extremes defined by conducting elements arranged in series and by conducting elements arranged in parallel. In a more recent landmark paper, Hashin and Shtrikman (1962) developed more restrictive bounds than the series and parallel limits and showed that their bounds were the most restrictive possible, when given only individual phase conductivities and volume fractions. Actually, the bounds given by Hashin and Shtrikman (1962) are too restrictive to rigorously apply to heterogeneous geologic formations because they were derived strictly for an isotropic medium.

Davis (1984) found that a weighted average of series and parallel conductive elements closely predicts the effective thermal conductivity of a rock matrix from the proportions and conductivities of the individual mineral constituents in the rock. Similarly, the overall rock conductivity is predicted from the void space with a fluid conductivity different from the rock matrix. The method of Davis (1984) is detailed in the following section.

Rock Matrix Conductivities

The expression for a weighted average of parallel and series conductive elements may be written as follows,

$$K = f\Sigma x_i K_i + (1 - f)\{\Sigma(x_i/K_i)\}^{-1} \quad (15)$$

where x_i is the volume fraction of individual mineral components constituting the rock matrix, Ki (mcal/s/cm/K) is the thermal conductivity of a mineral component at room temperature (298 K), and f is an empirically adjusted weighting factor which gives the best agreement between the predicted thermal conductivity and the experimentally observed value. The value of f cannot be accurately determined because of the range in conductivities ascribed to individual mineral components. However, using the data of Birch and Clark (1940) for rocks of known mineral content and the mineral component conductivities from Horai (1971), f is calculated to be about 0.3. Therefore, equation (15) may be replaced by

$$K_g = 0.3\Sigma x_i K_i + 0.7\{\Sigma x_i/K_i)\}^{-1} \quad (16)$$

An approximate empirical expression for the temperature dependence of thermal conductivities of rocks and minerals is given by

$$R = a_0 + a_1 T^{\lambda} \quad (17)$$

where R is the thermal resistivity of the mineral component (equal to $1000/K_g$), λ is an adjustable power, T is the temperature in kelvins, and a_0 and a1 are the intercept and slope characteristic of the particular rock matrix or mineral component. This expression for temperature dependence is valid for most applications in sedimentary basins. A value of $\lambda = 0.5$ adequately fits most experimental data. Both positive and negative slopes are observed with these plots, and the slopes and intercepts are directly related to each other in a linear fashion. Substituting these relations into equation (17) leads to a general expression for the temperature dependence of the thermal conductivity of rock matrix in terms of the conductivity at 298 K, as in

$$K_g(T) = [K_g^{-1}(2.412 - 0.0818T^{0.5}) + 0.01724T^{0.5} - 0.2978]^{-1} \quad (18)$$

Thermal Conductivity of Pore Fluid

The effective thermal conductivity of pore fluid is subject to an additional mixture rule if multiple saturations exist within the rock void space. The present case is simplified since it is assumed that the only fluid phase is water. Although the thermal conductivity of water is dependent on the concentration of dissolved ions and on temperature, there is no correction here for dissolved ions since their concentrations are not known. Several algorithms have been used to describe the thermal conductivity of water. All useful expressions must address the fact that the thermal conductivity of water passes through a maximum at about 150°C (423 K). A particularly simple expression which represents the experimental data for water up to about 325°C and which is adequate for our purposes here is given by

$$K_w(T) = 2.231(T/T_0)^{1.5} - 8812(T/T_0)^{2.5} \quad (19)$$

where K_w is in mcal/s /cm/K, T is in kelvins, and $T_0 = 273.2$ K

Thermal Conductivity of Porous Water-Saturated Rock

The remaining task is to provide an estimate of the effective thermal conductivity of a water-saturated rock. Equation (15) is again used for this estimate, except that $f = 0.5$ is substituted. This value is based on somewhat limited evidence, but it provides very good results in most cases. An ideal test of this relation requires a series of porous rocks with widely varying porosities but which have identical grain conductivities and are saturated with the same fluid. One close approximation to this situation is provided by a suite of vesicular basalts having very similar grain conductivities (Robertson and Peck, 1974). The morphology of the void spaces in these rocks is undoubtedly somewhat different from that in sedimentary rocks, but the effective conductivity should not be highly dependent on morphological differences, unless there is a large percentage of pores which is inaccessible to the pore fluid. The conductivity measurements on these basalts is fit quite well using a value of $f = 0.5$. Equation (15) thus becomes

$$K_R = 0.5\{\phi Kf + (1 - \phi)K_g\} + 0.5\{\phi/K_f + (1 - \phi)/K_g\}^{-1} \quad (20)$$

where K_R is the conductivity of the saturated rock, Kf is the saturating fluid conductivity, K_g is the grain conductivity, and ϕ is the porosity of the rock.

The methods developed here allow approximation of effective thermal conductivities of water-saturated rocks whenever the porosity and mineral composition are known. Such approximations are quite useful in modeling thermal processes in sedimentary basins, such as the application given in this paper.

REFERENCES CITED

Bathurst, R. G. C., 1975, Carbonate sediments and their diagenesis: Amsterdam, Elsevier, 658 p.

Beck, A. E., 1988, Methods for determining thermal conductivity and thermal diffusivity, *in* R. Haenel, L. Rybach, and L. Stegena, eds., Handbook of terrestrial heat-flow density determination: Dordrecht, Kluwer Academic, p. 87–124.

Birch, F., and H. Clark, 1940, The thermal conductivity of rocks and its dependence upon temperature and composition: American Journal of Science, v. 238, p. 529–558.

Blackwell, D. D., 1978, Heat flow and energy loss in the western U.S, *in* R. B. Smith and G. P. Eaton, eds., Cenozoic tectonics and regional geophysics of the Western Cordillera: Geological Society of America Memoir 152, p. 175–208.

Bredehoeft, J. D., R. D. Djevanshir, and K. R. Belitz, 1988, Lateral fluid flow in a compacting sand-shale sequence: South Caspian basin: AAPG Bulletin, v. 72, p. 416–424.

Clark, K. F., 1982, Mineral composition of rocks, *in* R. S. Carmichael, ed., Handbook of physical properties of rocks: Boca Raton, Florida, CRC, p. 1–216.

Davis, B. W., 1984, Thermal conductivities of reservoir rocks: Chevron Oil Field Research Company internal company technical memorandum, 32 p.

Freeze, R. A., and J. A. Cherry, 1979, Groundwater: Englewood Cliffs, New Jersey, Prentice-Hall, 604 p.

Hanshaw, B. B., and J. D. Bredehoeft, 1968, On the maintenance of anomalous fluid pressures: II. source layer at depth: Geological Society of America Bulletin, v. 79, p. 1107–1122.

Hardie, L. A., 1967, The gypsum-anhydrite equilibrium at one atmosphere pressure: American Mineralogist, v. 52, p. 171–200.

Hashin, Z., and S. Shtrikman, 1962, A variational approach to the theory of the effective magnetic permeability of multiphase materials: Journal of Applied Physics, v. 33, p. 3125–3131.

Horai, K., 1971, Thermal conductivity of rock-forming minerals: Journal of Geophysical Research, v. 76, p. 1278–1308.

Jarvis, G. T., 1984, An extensional model of graben subsidence—the first stage of basin evolution: Sedimentary Geology, v. 40, p. 13–31.

Jowett, E. C., 1991, Post-collisional formation of the Alpine foreland rifts: Annales Societatis Geologorum Poloniae, v. 61, p. 37–59.

Jowett, E. C., and G. T. Jarvis, 1984, Formation of foreland rifts: Sedimentary Geology, v. 40, p. 51–72.

MacDonald, G. J. F., 1953, Anhydrite-gypsum equilibrium relations: American Journal of Science, v. 251, p. 884–898.

Maxwell, J. C., 1891, A Treatise on electricity and magnetism (1954 reprint): New York, Dover, v. 1, 506 p.

Murray, R. C., 1964, Origin and diagenesis of gypsum and anhydrite: Journal of Sedimentary Petrology, v. 34, p. 512–523.

Pollack, H. N., and K. R. Cercone, 1988, Are anomalous thermal maturities in sedimentary basins due to the low thermal conductivity of carbonaceous deposits? (abs.): GSA Abstracts with Programs, v. 20, p. A259.

Robertson, E. C., and D. L. Peck, 1974, Thermal conductivity of vesicular basalt from Hawaii: Journal of Geophysical Research, v. 79, p. 4875–4888.

Rouchy, J. M., A. Laumondais, and E. Groessens, 1987, The Lower Carboniferous (Visean) evaporites in northern France and Belgium: depositional, diagenetic and deformational guides to reconstruct a disrupted evaporitic basin, *in* T. M. Peryt, ed., Evaporite basins: Berlin, Springer-Verlag, p. 31–67.

Roy, R. F., A. E. Beck, and Y. S. Touloukian, 1981, Thermophysical properties of rocks, *in* Y. S. Touloukian, W. R. Judd, and R. F. Roy, eds., Physical properties of rocks and minerals: New York, McGraw-Hill, p. 409–502.

Schreiber, B. C., 1978, Environments of subaqueous gypsum deposition, *in* W. E. Dean and B. C. Schreiber, eds., Marine evaporites: SEPM Short Course 4, p. 43–73.

Schuhmeister, J., 1877, Versuche über das Wärmeleitungsvermögen der Baumwolle, Schafwolle und Seide: Sitzungsberichte der Mathematisch-Naturwissenschaftlichen Klasse der Kaiserlichen Akademie der Wissenschaften, Wein, v. 76, p. 283.

Sclater, J. G., and P. A. F. Christie, 1980, Continental stretching: an explanation of the post-mid-Cretaceous subsidence of the central North Sea basin: Journal of Geophysical Research, v. 85, p. 3711–3739.

Shearman, D. J., 1963, Recent anhydrite, gypsum, dolomite, and halite from the coastal states of the Arabian shore of the Persian Gulf (abs.): Proceedings of the Geological Society of London, no. 1607, p. 63–65.

Sonnenfeld, P., 1984, Brines and evaporites: Orlando, Florida, Academic Press, 613 p.

Zen, E-an, 1965, Solubility measurements in the system $CaSO_4$-$NaCl$-H_2O at 35°, 50°, and 70°C and one atmosphere pressure: Journal of Petrology, v. 6, p. 124–164.